

**Single- and double-electron-capture processes in the collisions of C<sup>4+</sup> ions with He**L. L. Yan,<sup>1</sup> Y. Wu,<sup>1</sup> Y. Z. Qu,<sup>2</sup> J. G. Wang,<sup>1</sup> and R. J. Buenker<sup>3</sup><sup>1</sup>*Data Center for High Energy Density Physics, Institute of Applied Physics and Computational Mathematics, P.O. Box 8009, Beijing 100088, China*<sup>2</sup>*College of Material Sciences and Optoelectronic Technology, Graduate University of the Chinese Academy of Sciences, P.O. Box 4588, Beijing 100049, China*<sup>3</sup>*Fachbereich C-Mathematik und Naturwissenschaften, Bergische Universität Wuppertal, D-42097 Wuppertal, Germany*  
(Received 11 May 2013; published 19 August 2013)

The nonradiative single-electron-capture (SEC) and double-electron-capture (DEC) processes for C<sup>4+</sup>(1s<sup>2</sup>) colliding with He atoms are investigated by using the quantum-mechanical molecular-orbital close-coupling method. Total and state-selective electron-capture cross sections are calculated in the energy range of 10<sup>-6</sup>–6 keV/amu. For energies less than 2 keV/amu, the DEC dominates the electron-capture processes. As the energy increases, the SEC cross sections increase while the DEC cross sections decrease; when  $E > 2$  keV/amu, the SEC process becomes the dominant mechanism. It is found that the SEC processes mainly result from the electron capture to  $n = 3$  channels of C<sup>3+</sup> ion for energy below 0.7 keV/amu and from  $n = 2$  channels for  $E > 0.7$  keV/amu. Compared with the available theoretical calculations, better agreement is achieved between the present results and the available measurements for total DEC and SEC cross sections. For state-resolved cross sections, excellent agreement is obtained for two-electron capture to C<sup>2+</sup>(2s<sup>2</sup>), C<sup>2+</sup>(2s2p), and C<sup>2+</sup>(2p<sup>2</sup>) and one-electron capture to C<sup>3+</sup>(2s) and C<sup>3+</sup>(2p) between the present calculations and the available theoretical and experimental results.

DOI: [10.1103/PhysRevA.88.022706](https://doi.org/10.1103/PhysRevA.88.022706)

PACS number(s): 34.70.+e, 34.20.-b

**I. INTRODUCTION**

Electron-capture processes by carbon ions colliding with atoms or molecules are of great interest in magnetic confined fusion plasma and have been investigated extensively. Carbon ions are important plasma constituents and impurities in fusion research devices since carbon is used in divertor target plates. As the product of fusion production, helium is also important in the fusion plasma environment. C<sup>4+</sup> + He collisions have been studied intensively in both experimental and theoretical investigations. Zwally *et al.* [1] have measured single-electron-capture (SEC) cross sections in the energy region of 1–2 keV/amu by using a spark source of C<sup>4+</sup> ions. Crandall *et al.* [2,3] have studied the single- and double-electron-capture processes in C<sup>4+</sup> collisions with He and found that double-electron capture (DEC) dominates the electron-capture processes in the low-collision-energy region and DEC cross sections are nearly two orders larger than SEC cross sections. By means of optical spectroscopy, the  $n, l$ -resolved SEC cross sections were determined by Dijkkamp *et al.* [4] for energies from 0.83 to 6.67 keV/amu. Ishii *et al.* [5] investigated the electron capture in C<sup>4+</sup> + He collisions for energies less than 0.6 keV/amu by using a mini-electron-beam ion-source apparatus in combination with an octopole-ion-beam-guide technique. They also calculated the electron-capture cross sections for the energy range of 0.1–5 keV/amu by using the classical-over-the-barrier (COB) model method. However, significant discrepancies exist between their experimental and theoretical results. Shipsey *et al.* [6] studied both the SEC and DEC processes in the energy range of 0.2–8.0 keV/amu by using the semiclassical molecular-orbital close-coupling (SMOCC) method. The DEC cross sections obtained are in good agreement with the experimental measurements of Crandall *et al.* [2], but their SEC cross sections are much smaller than the measurements of Ishii *et al.* [5]. By using

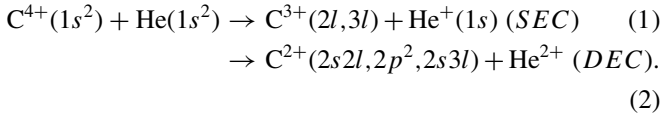
the SMOCC method, Kimura and Olson [7] also computed the total SEC and DEC cross sections for energies from 0.06 to 8.0 keV/amu. For energies less than 0.4 keV/amu, the DEC cross sections display a tendency consistent with the experimental work of Phaneuf and Crandall [8] and their SEC cross sections also agree well with the measurements of Ishii *et al.* [5]. Subsequently, Errea *et al.* [9,10] studied C<sup>4+</sup> + He collisions, for which both the total and state-selective cross sections were calculated for SEC and DEC processes in the energy range of 0.4–6.0 keV/amu. They found a sharp maximum in DEC cross sections at 60 eV/amu. It is interesting that they found that the SEC cross sections increase with decreasing energy, in contrast to other findings [5,7,8]. Hansen [11] applied the atomic orbital close-coupling (AOCC) method to study C<sup>4+</sup> + He collisions and the total SEC and DEC cross sections were obtained in the energy range of 0.05–4.00 keV/amu, in which the DEC cross sections are slightly smaller than the measurements [2,5] for  $E > 2$  keV/amu and the SEC results are nearly constant for  $E < 0.3$  keV/amu. In a recent AOCC investigation Zhao *et al.* [12] computed the state-selective SEC cross sections and polarization degree for the  $3p^2P_{3/2}-3s^2S_{1/2}$  transition of C<sup>3+</sup>(3p) in the energy range of 1–7 keV/amu and provided information about electron capture to different magnetic substates. Pichl *et al.* [13] have studied double-electron-capture differential cross sections for collision energies at 270, 400, and 470 eV based on an *ab initio* treatment of electronic states [14]. Using quantum-mechanical four-body distorted-wave theories, the DEC processes in collisions between multiply charged ions and heliumlike atomic systems have been investigated by Belkić *et al.* [15,16].

Despite the intensive investigation of C<sup>4+</sup> + He collisions that have been performed using both theory and experiment, larger discrepancies exist in the available experimental and calculated results. Furthermore, these studies mainly focused on C<sup>4+</sup> + He collisions for energies larger than 50 eV/amu.

TABLE I. Asymptotic separated-atom energies for the states of  $\text{CHe}^{4+}$ .

Molecular states	Asymptotic atomic states	Ref. [22]	Energy ( $\text{cm}^{-1}$ )	
			MRD-CI	Error
1 $^1\Sigma^+$	$\text{C}^{3+}(1s^2 2s^2 \text{S}) + \text{He}^+(1s)$	0	0	0
2 $^1\Sigma^+$	$\text{C}^{2+}(1s^2 2s^2 \text{S}) + \text{He}^{2+}$	52668	52620	48
3 $^1\Sigma^+, 1^1\Pi$	$\text{C}^{3+}(1s^2 2p^2 \text{P}^0) + \text{He}^+(1s)$	64538	64467	71
4 $^1\Sigma^+, 2^1\Pi$	$\text{C}^{2+}(1s^2 2s 2p^1 \text{P}^0) + \text{He}^{2+}$	155020	155071	51
5 $^1\Sigma^+, 3^1\Pi, 1^1\Delta$	$\text{C}^{2+}(1s^2 2p^2 \text{D}) + \text{He}^{2+}$	198544	198386	158
6 $^1\Sigma^+$	$\text{C}^{2+}(1s^2 2p^2 \text{S}) + \text{He}^{2+}$	235188	235367	179
7 $^1\Sigma^+$	$\text{C}^{3+}(1s^2 3s^2 \text{S}) + \text{He}^+(1s)$	302849	302466	383
8 $^1\Sigma^+$	$\text{C}^{2+}(1s^2 2s 3s^1 \text{S}) + \text{He}^{2+}$	299838	299712	126
9 $^1\Sigma^+$	$\text{C}^{4+}(1s^2 \text{S}) + \text{He}(1s^2)$	321868	321405	463
10 $^1\Sigma^+, 4^1\Pi$	$\text{C}^{2+}(1s^2 2s 3p^1 \text{P}^0) + \text{He}^{2+}$	311599	311162	437
11 $^1\Sigma^+, 5^1\Pi$	$\text{C}^{3+}(1s^2 3p^2 \text{P}^0) + \text{He}^+(1s)$	320066	319828	238
12 $^1\Sigma^+, 6^1\Pi, 2^1\Delta$	$\text{C}^{3+}(1s^2 3d^2 \text{D}) + \text{He}^+(1s)$	324885	324319	566
13 $^1\Sigma^+, 7^1\Pi, 3^1\Delta$	$\text{C}^{2+}(1s^2 2s 3d^1 \text{D}) + \text{He}^{2+}$	329151	329304	153

In order to resolve the discrepancy between the measurements and calculations in  $\text{C}^{4+} + \text{He}$  collisions, as well as study the collision dynamics in the very-low-energy range, a quantum-mechanical molecular-orbital close-coupling (QMOCC) method is utilized to investigate the following processes:



The adiabatic potentials and radial and rotational coupling matrix elements used in the QMOCC calculations have been computed by using the *ab initio* multireference single- and double-excitation configuration-interaction (MRD-CI) method. Total and state-selective SEC and DEC cross sections have been calculated and compared with the available theoretical and experimental results. Section II describes the calculation of the molecular potential and couplings utilized in the present QMOCC calculations. Section III discusses the QMOCC method briefly. Section IV presents the results of the scattering calculation. A brief summary is given in Sec. V. Atomic units are used throughout unless otherwise noted.

## II. ELECTRONIC STRUCTURE CALCULATIONS

In the present study, the multireference configuration-interaction (CI) calculations have been carried out for adiabatic potential energies of the lowest thirteen  $^1\Sigma^+$  states, the lowest three  $^1\Delta$  states in  $A_1$  ( $C_{2v}$ ) symmetry, and the lowest seven  $^1\Pi$  states in  $B_1$  symmetry of the  $\text{CHe}^{4+}$  system by employing the MRD-CI package [17,18]. All electrons, not only the valence ones, are included in the present CI calculation. For carbon and helium atoms, the correlation-consistent polarized valence quadruple-zeta cc-pVQZ Gaussian basis sets [19,20] have been used. Besides the above basis, the  $(1s, 1p, 1d)$  diffuse functions are added to describe the Rydberg states of the carbon atoms. The  $(13s, 7p, 4d, 2f, 1g)$  basis set contracted to the  $[6s, 5p, 4d, 2f, 1g]$  basis set [19] is employed for carbon and the  $(7s, 3p, 2d, 1f)$  basis set contracted to the  $[4s, 3p, 2d, 1f]$  basis set [20] is employed for helium. A threshold of  $10^{-10}$

hartree was used to select the configurations [18,21] of  $\text{CHe}^{4+}$  molecular ions for internuclear distances from 0.5 to 50 a.u. The spin-orbit interactions are neglected in our calculations since their effects are small and within the numerical error range. As shown in Table I, the relative errors between the calculated energies and the experimental atomic energies [22] are less than  $566 \text{ cm}^{-1}$  (0.07 eV) in the asymptotic region. This accuracy level is adequate for treating the present dynamics of  $\text{C}^{4+} + \text{He}$  collisions [9,23].

As shown in Fig. 1, the calculated adiabatic potential-energy curves for the lowest thirteen  $^1\Sigma^+$ , seven  $^1\Pi$ , and three  $^1\Delta$  molecular states of  $\text{CHe}^{4+}$  have been presented as a function of internuclear distance. The numbering of the states has been taken from their ordering at  $R = 50$  a.u. Note that some sharp avoided crossings have been replaced by real crossings, including the one between the 5  $^1\Sigma^+$  and 9  $^1\Sigma^+$  states at  $R \sim 7.16$  a.u. and the one between the 6  $^1\Sigma^+$  and 9  $^1\Sigma^+$  states at  $R \sim 10.2$  a.u. in the internuclear distance region for  $R < 15$  a.u. Due to the diabatic feature of the couplings, the transitions induced by them are negligible compared to those involving other couplings in the energy range considered. In all, twenty (thirteen  $^1\Sigma^+$  and seven  $^1\Pi$ ) molecular states are considered in the scattering calculations, including the initial, SEC, and DEC channels. The 9  $^1\Sigma^+$  state represents the initial channel for our considered  $\text{C}^{4+}(1s^2) + \text{He}(1s^2)$  collision processes and only the singlet states are involved in the collision dynamics. The DEC channels dissociate to  $\text{C}^{2+}(2s^2)$ ,  $\text{C}^{2+}(2s 2p)$ , and  $\text{C}^{2+}(2p^2)$  states that lie close to the initial channel, while the SEC channels dissociate to  $\text{C}^{3+}(2l)$  ( $l = s, p$ ) and  $\text{C}^{3+}(3l)$  ( $l = s, p, d$ ) states that are relatively far away from the initial channel.

The coupling matrix elements can be separated into radial and rotational terms that describe the  $^1\Sigma^+ \rightarrow ^1\Sigma^+$  ( $^1\Pi \rightarrow ^1\Pi$ ) and  $^1\Sigma^+ \rightarrow ^1\Pi$  transitions, respectively. The adiabatic radial coupling elements are calculated by using a finite-difference approximation

$$A_{ij}^R = \langle \psi_i | \frac{\partial}{\partial R} | \psi_j \rangle = \lim_{\Delta R \rightarrow 0} \frac{1}{\Delta R} \langle \psi_i(R) | \psi_j(R + \Delta R) \rangle \quad (3)$$

with a step size of 0.0002 a.u. Figures 2(a)–2(c) display the nonadiabatic radial coupling matrix elements. The positions

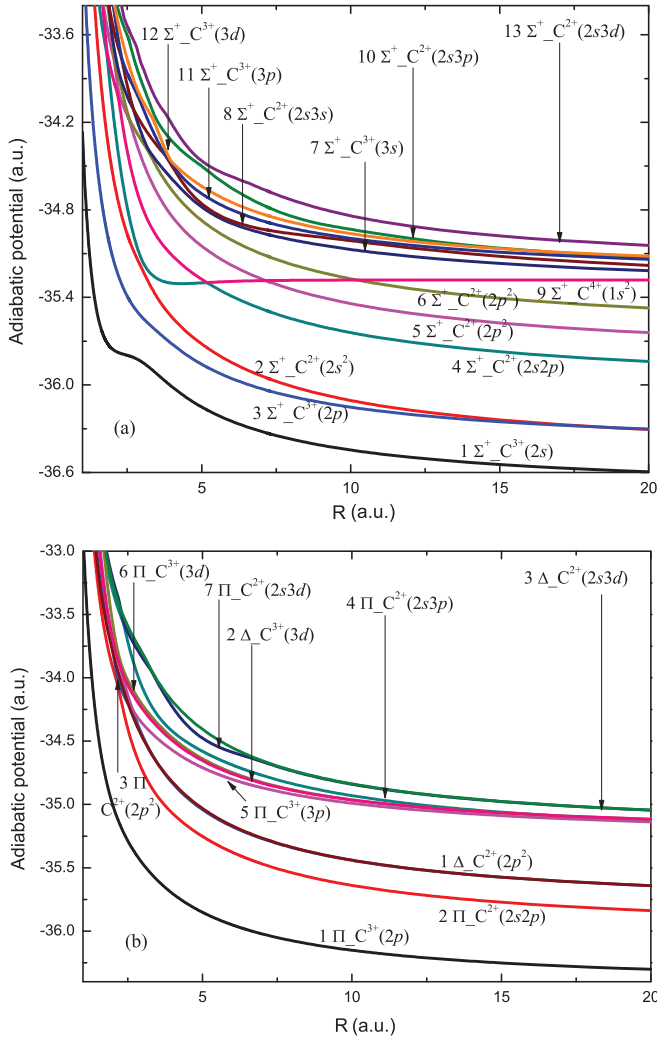


FIG. 1. (Color online) Adiabatic potential curves for  $\text{CHe}^{4+}$  as a function of internuclear distance.

of the peaks in the radial couplings are consistent with the avoided crossings of the adiabatic potentials. From Fig. 2(a) one can see that the initial  $9^1\Sigma^+$  state is strongly coupled with the  $4^1\Sigma^+$  state at  $R \sim 5.18$  a.u., with a unit transition probability. There is a broad peak centered at  $R \sim 3.0$  a.u. in the physically important  $2^1\Sigma^+-4^1\Sigma^+$  radial coupling, which drives the transitions to the main double-electron-capture  $\text{C}^{2+}(2s^2)$  channel. For smaller internuclear separations  $R < 4$  a.u. it is obvious that the sharp peaks exist in the series of  $5^1\Sigma^+-6^1\Sigma^+-7^1\Sigma^+-8^1\Sigma^+-10^1\Sigma^+-11^1\Sigma^+-12^1\Sigma^+$  radial coupling matrix elements, which will therefore play a significant role in the collision dynamics for transitions to the states dissociating to  $\text{C}^{3+}(3l)$  channels in the relatively-low-energy region.

Some important adiabatic rotational coupling matrix elements  $A_{ij}^\theta = \langle \psi_i | iL_y | \psi_j \rangle$  are presented in Fig. 2(d). These couplings drive the transitions between states of the same spin but of different spatial symmetry. Due to the strong adiabatic interactions between the adjacent states, the rotational couplings are not smooth near the positions of avoided crossings. The initial  $9^1\Sigma^+$  state is rotationally strongly coupled to the

$2^1\Pi$  state corresponding to the electron-capture channel to  $\text{C}^{2+}(2s2p) + \text{He}^{2+}$ .

In Fig. 3 the comparisons of the present couplings with those of Errea *et al.* [10] are presented. In the work of Errea *et al.* [10], the sharp avoided crossings between  $4^1\Sigma^+-9^1\Sigma^+$  at  $R \sim 5.20$  a.u. have been replaced by real crossings. For the convenience of comparison, the present ordering has been applied. In Fig. 3(a) the dominant radial couplings between  $2^1\Sigma^+-3^1\Sigma^+$ ,  $2^1\Sigma^+-4^1\Sigma^+$ ,  $3^1\Sigma^+-9^1\Sigma^+$ ,  $6^1\Sigma^+-7^1\Sigma^+$ , and  $5^1\Sigma^+-9^1\Sigma^+$  are displayed and compared with the results of Errea *et al.* It can be observed that there is excellent agreement between the two calculations in the entire  $R$  range for  $2^1\Sigma^+-3^1\Sigma^+$ ,  $2^1\Sigma^+-4^1\Sigma^+$ , and  $3^1\Sigma^+-9^1\Sigma^+$  radial couplings, as well as for  $6^1\Sigma^+-7^1\Sigma^+$  and  $5^1\Sigma^+-9^1\Sigma^+$  couplings when  $R > 2.1$  a.u. However, significant differences appear for  $6^1\Sigma^+-7^1\Sigma^+$  and  $5^1\Sigma^+-9^1\Sigma^+$  radial couplings for smaller  $R$ . For the  $6^1\Sigma^+-7^1\Sigma^+$  coupling, a new coupling is obtained at  $R \sim 1.97$  a.u., which decreases the probability of single-electron capture to the  $\text{C}^{3+}(3l)$  channel. For  $5^1\Sigma^+-9^1\Sigma^+$  coupling, one more sharp peak at  $R \sim 1.6$  a.u. is obtained. These discrepancies in the small- $R$  range are possibly caused by the effective two-active-electron approximation adopted in the calculation of Errea *et al.* [10]. For the rotational couplings of  $2^1\Sigma^+-1^1\Pi$ ,  $3^1\Sigma^+-1^1\Pi$ ,  $4^1\Sigma^+-1^1\Pi$ , there is good agreement between the present calculations and the ones of Errea *et al.*, as shown in Fig. 3(b).

### III. THEORETICAL METHOD

The cross sections for ion-atom collisions are calculated in this work by using the QMOCC method formulated and described thoroughly by Zygelman and Dalgarno [24] and Kimura and Lane [25]. Here we only discuss it briefly. It involves solving a coupled set of second-order differential equations by using the log-derivative method [26]. Its solutions are the scattering amplitudes of the total system wave function expanded over a truncated set of molecular eigenfunctions. In the adiabatic representation, transitions between channels are driven by elements (radial  $A^R$  and rotational  $A^\theta$ ) of the vector potential  $A(\vec{R})$ , where  $\vec{R}$  is the internuclear distance vector. Since the adiabatic description contains first-order derivatives, it is numerically convenient to make a unitary transformation [24,27] to a diabatic representation

$$U(R) = W(R)[V(R) - P(R)]W^{-1}(R), \quad (4)$$

where  $U(R)$  is the diabatic potential matrix,  $V(R)$  is the diagonal adiabatic potential,  $W(R)$  is a unitary transformation matrix, and  $P(R)$  is the rotational matrix of the vector potential  $A(\vec{R})$ .

The charge-capture cross section from the initial channel  $i$  to the final channel  $j$  is given by

$$\sigma_{(i \rightarrow j)} = \frac{\pi}{k_i^2} \sum_J (2J+1) |S_J|_{i,j}^2, \quad (5)$$

where  $k_i$  is the initial momentum,  $J$  is the total angular momentum, and  $S$  is the scattering matrix

$$S_J = [I + iK_J]^{-1}[I - iK_J], \quad (6)$$

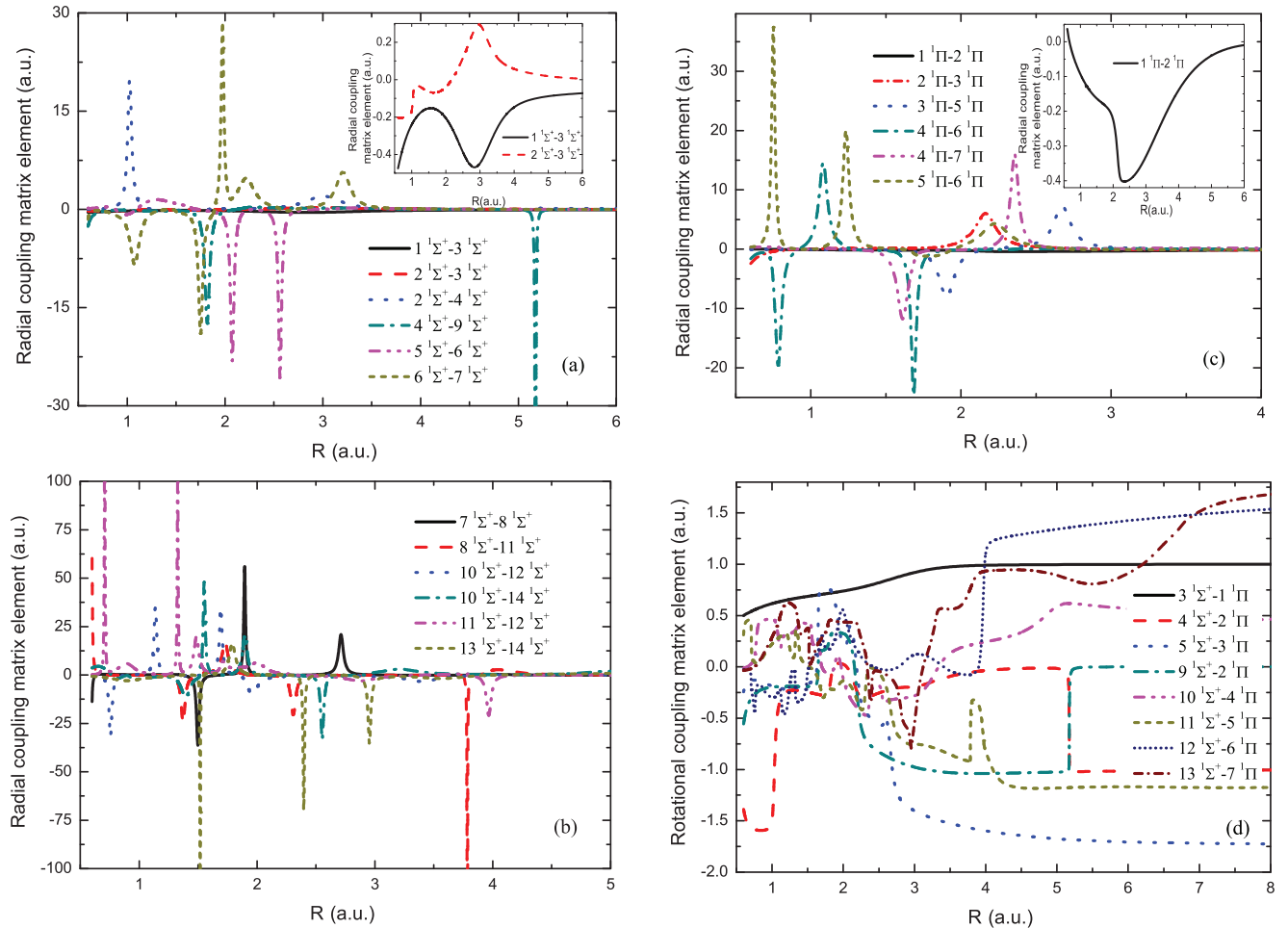


FIG. 2. (Color online) Coupling matrix elements for  $\text{CHE}^{4+}$ : (a) and (b) radial coupling matrix element between  $1\Sigma^+$  states, (c) radial coupling matrix element between  $1\Pi$  states, and (d) rotational coupling matrix element between  $1\Sigma^+$  and  $1\Pi$  states.

where  $I$  is the identity matrix and the  $K$  matrix is obtained from the scattering amplitude after a partial-wave decomposition [24]. In the present work, electron translation factors (ETFs) [28], which are often used to modify the molecular eigenfunctions to remove asymptotic couplings between atomic states, are not included. This constitutes a limitation of the present findings in the light of the anticipated importance of this effect in the higher-energy range for  $E > 1$  keV/amu.

#### IV. RESULTS AND DISCUSSION

The QMOCC method has been applied to investigate  $\text{C}^{4+}(1s^2)$  collisions with He and the SEC and DEC cross sections have been obtained for a wide energy range of  $10^{-6}$ –6 keV/amu, as shown in Fig. 4. For the energy range of  $5 \times 10^{-4}$ –6 keV/amu, 20 channels have been considered in the calculation, including thirteen  $1\Sigma^+$  states and seven  $1\Pi$  states; for lower incident energies of  $10^{-6}$ – $10^{-3}$  keV/amu, higher-lying channels are closed and only 12 channels have been considered in the calculation, including nine  $1\Sigma^+$  states and three  $1\Pi$  states. Excellent agreement has been obtained between the two calculations in the energy region of  $5 \times 10^{-4}$ – $10^{-3}$  keV/amu, which demonstrates that the contributions from those higher-lying channels can be neglected. It can be

observed in Fig. 4 that DEC dominates the collision processes, except that SEC and DEC cross sections become comparable for incident energy larger than 1 keV/amu, which is consistent with previous experimental and theoretical studies [2,3,5–11]. The DEC processes occur mainly through transitions at the avoided crossing between the  $2^1\Sigma^+$  and  $4^1\Sigma^+$  states near  $R \sim 3.0$  a.u. The SEC process takes place through a basic mechanism in which single-transfer states are populated from double-transfer channels. For example, the avoided crossings of  $5^1\Sigma^+-9^1\Sigma^+$ ,  $5^1\Sigma^+-6^1\Sigma^+$ , and  $6^1\Sigma^+-7^1\Sigma^+$  shown in Figs. 2(a) and 3(a) indicate that an electron is first transferred from the initial  $9^1\Sigma^+$  state to the  $\text{C}^{2+}(2p^2)$  channels and this is followed immediately by transition to the  $\text{C}^{3+}(3s)$  exit channel. The total SEC and DEC cross sections both have minima near 1 eV/amu and then the DEC cross sections increase slowly to a local maximum at about 0.1 keV/amu, while the SEC cross sections keep increasing up to the largest energy studied of 6 keV/amu. For energies less than 1 eV/amu, the QMOCC results display Langevin behavior, where the polarization interaction dominates the electron-capture processes. Remarkable oscillation structures, appearing in both the SEC and DEC cross sections for  $E < 1.0$  eV/amu, are attributed to the presence of quasibound rotational-vibrational states of the intermediate molecular complex formed temporarily from  $\text{C}^{4+}$

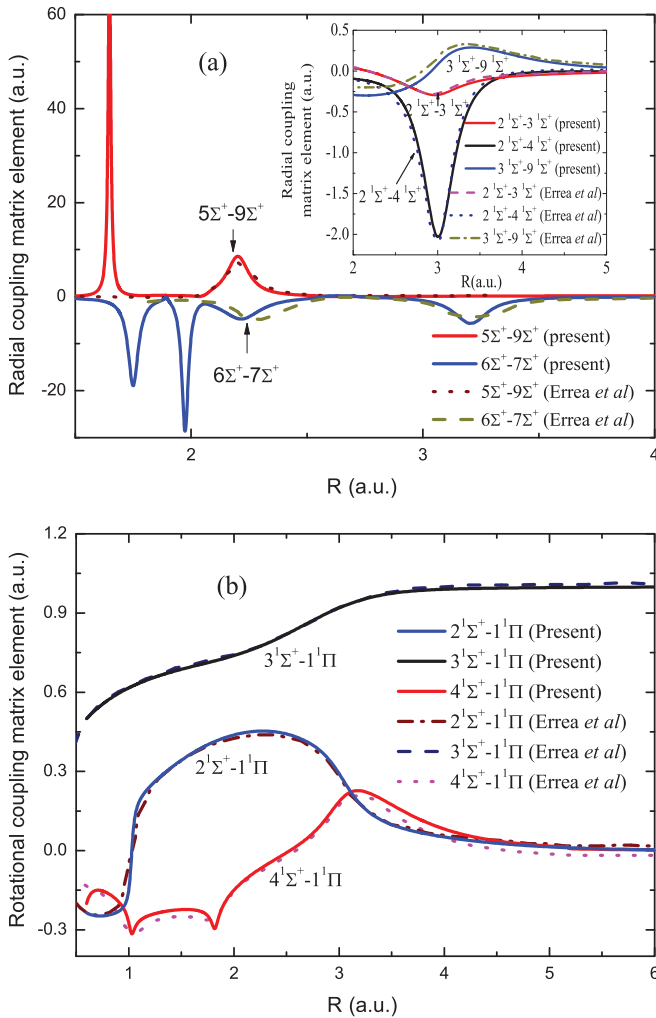


FIG. 3. (Color online) Comparison of the present couplings for  $\text{CHe}^{4+}$  with those of Errea *et al.* [10]: (a) radial couplings and (b) rotational couplings.

and He in the entrance channel [29–31]. For both sharp and broad resonances, there is a certain partial wave  $J$  that makes

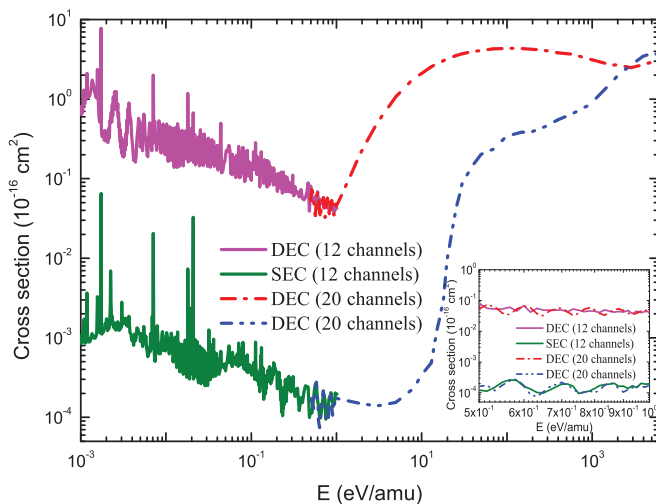


FIG. 4. (Color online) Comparison between the present total single- and double-electron-capture cross sections.

the major contribution to the resonance. Using the effective potential  $V_J^{\text{eff}}(R) = V(R) + J(J+1)/2\mu R^2$  of the entrance channel, one can obtain the vibrational quantum number. Similar resonance structures in the low-energy region for the radiative processes can also be identified by their rotational and vibrational quantum numbers [29–31]. As the collision energy increases, the effective angular momentum quantum numbers increase, which results in a shallower well of the effective potential, reducing the number of the quasibound vibrational states. In the following sections, the details of the DEC and SEC cross sections will be presented and compared with available experimental and theoretical results.

### A. Double-electron-capture cross sections

The present DEC cross sections are displayed in Fig. 5 and compared with available experimental [2,3,5,8] and theoretical [5–7,9–11] results. For clarification, the DEC and SEC cross sections are only presented and compared with available data in a limited energy region of 10 eV/amu to 6 keV/amu. In the overlapping energy region of 0.1–3 keV/amu, there is good agreement between the present QMOCC calculations and all data available in both trend and magnitude, except for the COB calculation of Ishii *et al.* [5], which is a simple classical model that overestimates the DEC cross sections. For energy less than 50 eV/amu, only Ishii *et al.* [5] have presented some DEC results. They obtained the experimental results by using a mini-electron-beam ion-source apparatus in combination with an octopole-ion-beam guide and have also computed the DEC cross sections by using the COB model. Large discrepancies exist between the present QMOCC results, the COB calculations of Ishii *et al.* [5], and their measurements. The present QMOCC data are about half as

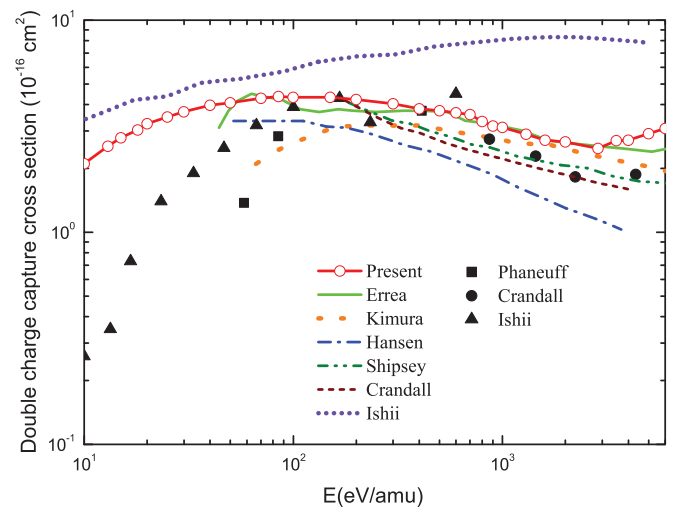


FIG. 5. (Color online) Comparison between the present DEC cross sections with other experimental and theoretical results. The theoretical results are from the present calculation (solid line with open circle), Errea *et al.* [9] (solid line), Kimura and Olson [7] (widely spaced short-dashed line), Hansen [11] (dash-dotted line), Shipsey *et al.* [6] (dash-double-dotted line), Crandall *et al.* [2] (short-dashed line), and Ishii *et al.* [5] (dotted line). The experimental results are from Phaneuff and Crandall [8] (solid squares), Crandall *et al.* [2] (solid circles), and Ishii *et al.* [5] (solid triangles).

large as the COB results, but they still greatly overestimate the measurements. This discrepancy may be due to angular scattering effects in the signal collection of the measurement, which tend to underestimate the absolute cross section for very low collision energies. For energy larger than 1 keV/amu, the present QMOCC results are larger than the calculations of Crandall *et al.* [2], Shipsey *et al.* [6], and Hansen [11] and about 50% larger than the measurements of Crandall *et al.* [2], but agree well with the calculations of Kimura and Olson [7] and Errea *et al.* [9,10], except for  $E > 3$  keV/amu. In the study of Errea *et al.*, the SMOCC method was applied and fourteen molecular channels were included in their calculation. The good agreement between the present QMOCC data and the SMOCC results of Errea *et al.* [9,10] is due to the fact that a similar molecular-orbital expansion method and couplings are used in the scattering calculation, as shown in the inset of Fig. 3(a). The small discrepancies between the present QMOCC results and the data of Errea *et al.* are also due to the small differences in the coupling calculations. For energies above 3 keV/amu, the present DEC cross sections are larger than the results of Errea *et al.*, which can be attributed to the fact that the ETF has not been included in the present QMOCC treatment, which possibly becomes important for higher-energy collisions.

State-resolved DEC cross sections are presented in Fig. 6 and compared with the only available data of Errea *et al.* [9]. It can be found that capture to the  $C^{2+}(2s^2)$  state dominates in the entire energy region considered because of the strong coupling between the  $2^1\Sigma^+$  and  $4^1\Sigma^+$  states at  $R \sim 3.0$  a.u., as shown in Fig. 2. The DEC processes take place through a simultaneous release of both electrons from a correlated initial state when the projectile perturbation becomes strong enough. It can be observed in Fig. 6(a) that there is good agreement between the present results and the data of Errea *et al.* [9] for electron capture to the  $C^{2+}(2s^2)$  and  $C^{2+}(2s2p)$  states, while there is a large discrepancy between these two calculations for electron capture to the  $C^{2+}(2p^2)$  state. The state-resolved cross sections for electron capture to  $C^{2+}(2s3l)$  are presented in

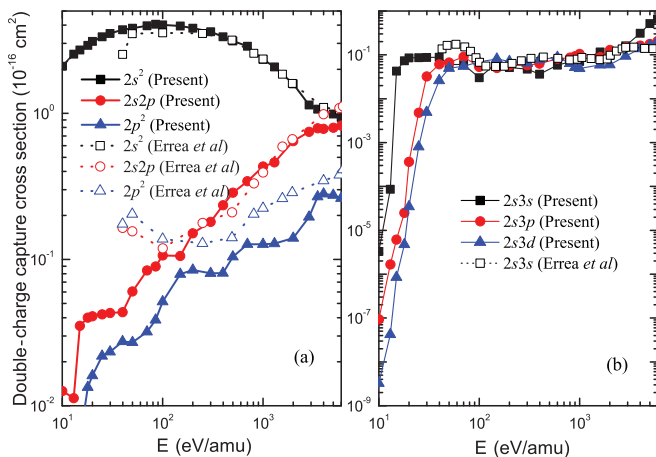


FIG. 6. (Color online) Comparison between state-selective DEC cross sections with the results of Errea *et al.* [9]: The present calculation is shown by the solid line with solid symbols and the results of Errea *et al.* [9] are shown by the dotted line with open symbols.

Fig. 6(b) and compared with the only  $C^{2+}(2s3s)$  result of Errea *et al.* [9]. It can be found that electron capture to  $C^{2+}(2s3l)$  states is not negligible and there is good agreement between the two calculations for electron capture to the  $C^{2+}(2s3s)$  state. It should be noted that all the endergonic channels for electron capture to  $C^{2+}(2s3l)$  states have been included in the present calculations, while only the  $C^{2+}(2s3s)$  channel has been considered in the treatment of Errea *et al.* [9]. Because of the strong-coupling effects between the  $C^{2+}(2s3l)$  and  $C^{2+}(2s2l)$  channels, there is a competitive mechanics between different electron-capture processes, which can easily explain the discrepancy for the  $C^{2+}(2p^2)$  cross section between our calculation and the one of Errea *et al.* For energy less than 100 eV/amu, the present cross sections for electron capture to the  $C^{2+}(2s2p)$  and  $C^{2+}(2p^2)$  states decrease as the energy decreases, which is opposite in trend to the results of Errea *et al.* The origin of this discrepancy is due to the model potential used in the structure calculation of Errea *et al.* [9], while a full-electron calculation has been performed within the present framework of the MRD-CI method.

### B. Single-electron-capture cross sections

The total SEC cross sections are presented in Fig. 7 and compared with available experimental [1–3,5,8,32] and theoretical [2–7,9–11] results in the energy range from 10 eV/amu to 6 keV/amu. Compared with the experimental data of Zwally *et al.* [1], Crandall *et al.* [2], Iwai *et al.* [32], Phaneuf and Crandall [8], and Dijkkamp *et al.* [4], the present QMOCC calculations merge into these measurements for energy larger

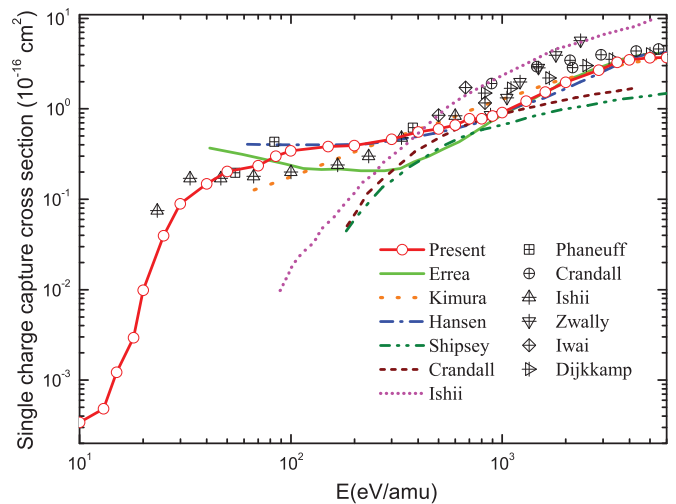


FIG. 7. (Color online) Comparison between the present SEC cross sections with other experimental and theoretical results. The theoretical results are from the present calculation (solid line with open circle), Errea *et al.* [9] (solid line), Kimura and Olson [7] (widely space short-dashed line), Hansen [11] (dash-dotted line), Shipsey *et al.* [6] (dash-double-dotted line), Crandall *et al.* [2] (short-dashed line), and Ishii *et al.* [5] (dotted line). The experimental results are from Phaneuf and Crandall [8] (crossed squares), Crandall *et al.* [2] (crossed circles), Ishii *et al.* [5] (crossed up-pointing triangles), Zwally *et al.* [1] (crossed down-pointing triangles), Iwai *et al.* [32] (crossed diamonds), and Dijkkamp *et al.* [4] (crossed right-pointing triangles).

than 200 eV/amu and lie between the results of Phaneuf and Crandall [8] and Ishii *et al.* [5] for lower energies. Compared with the available calculations, it is interesting that the present QMOCC calculations are in excellent agreement with the AOCC results of Hansen [11], except for  $E < 100$  eV/amu. It is well known that the AOCC method works well in treating one-electron processes in collisions of highly charged ions for energy larger than a few 100 eV/amu. For lower energy, AOCC does not work well due to the straight-line trajectory applied for nuclear motion. This is a further demonstration of the reliability of the present QMOCC calculations. The COB calculations of Ishii *et al.* [5] can just give some qualitative prediction of SEC cross sections for some energy range. Compared with the calculations of Shipsey *et al.* [6], Kimura and Olson [7], and Errea *et al.* [9], large discrepancies exist for energy less than 1 keV/amu. In these calculations [4,6,7,9], which are based on the molecular-orbital expansion method, the accuracy of the scattering cross section strongly depends on that of the molecular structure calculations and the molecular states included in the scattering calculation, which can explain the discrepancy for energy less than 1 keV/amu. In the present QMOCC calculation, all-electron calculations based on the MRD-CI method for potentials and couplings have been performed and all of the endergonic channels for an electron capture to  $C^{3+}(n=3)$  states have been included. In the calculation of Errea *et al.* [9], a model potential has been applied in the structure calculation and the endergonic channels of  $C^{3+}(3s)$  and  $C^{3+}(3p)$  have been included, while in the studies of Crandall *et al.* [2], Shipsey *et al.* [6], and Kimura and Olson [7] no endergonic channels of  $C^{3+}(n=3)$  have been included. The difference between the present  $6^1\Sigma^+-7^1\Sigma^+$  coupling and that of Errea *et al.* [10] shown in Fig. 3(a) provides information about the different charge-capture dynamics. The present  $6^1\Sigma^+-7^1\Sigma^+$  coupling centered at  $R \sim 2.2$  a.u. superposed by another sharp coupling leads to the present SEC cross sections slowly decreasing as the energies decrease.

In order to provide detailed information about the SEC processes,  $n$ -resolved and  $n,l$ -resolved SEC cross sections are presented and compared with available data in Figs. 8 and 9, respectively. In Fig. 8 the present QMOCC calculations show that electron capture to the  $n=3$  shell of  $C^{3+}$  dominates the SEC process for energy less than 700 eV/amu, while electron capture to the  $n=2$  shell of  $C^{3+}$  becomes more important for higher energies. For the process of electron capture to the  $n=3$  shell of  $C^{3+}$ , the transitions are driven through the series of  $5^1\Sigma^+-6^1\Sigma^+-7^1\Sigma^+-8^1\Sigma^+-10^1\Sigma^+-11^1\Sigma^+-12^1\Sigma^+$  strong avoided crossings around  $R \sim 3$  a.u., which are important in the energy range for  $E < 700$  eV/amu. Electron capture to the  $n=2$  shell of  $C^{3+}$  proceeds via transitions involving couplings among the  $1^1\Sigma^+$ ,  $2^1\Sigma^+$ ,  $3^1\Sigma^+$ , and  $4^1\Sigma^+$  states at small internuclear distance. For comparison, the total SEC cross sections for electron capture to  $C^{3+}(3s)$  and  $C^{3+}(3p)$  states obtained by Errea *et al.* [9] are also presented. The present QMOCC calculations and the results of Errea *et al.* [9] are in general agreement on the trends for cross sections for electron capture to the  $n=2$  and 3 shells of the  $C^{3+}$  ion, especially for energy larger than 0.7 keV/amu. The cross sections for electron capture to the  $n=3$  shell obtained by Errea *et al.* [9] resulting from the model potential

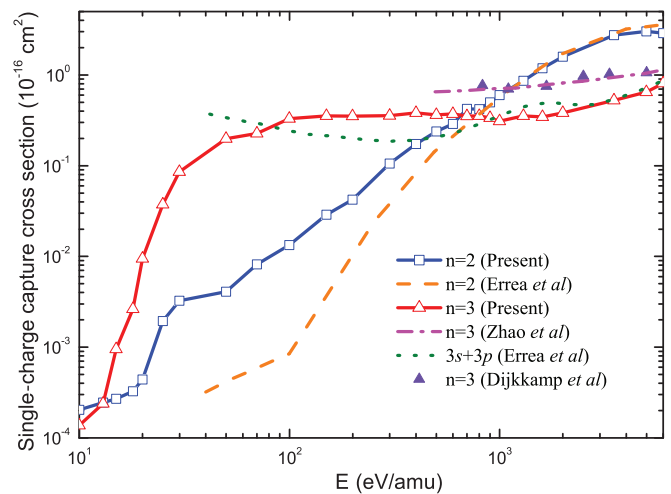


FIG. 8. (Color online) Comparison between the SEC cross sections for electron capture to the  $n=2$  and 3 shells of the  $C^{3+}$  ion with other theoretical and experimental results for  $C^{4+}(1s^2) + He$  collisions.

used in their structure calculations increase with decreasing energy. The present QMOCC calculations and SMOCC results of Errea *et al.* [9] for electron capture to the  $n=2$  shell of  $C^{3+}$  are smaller than the experimental measurements obtained by Dijkkamp *et al.* [4] and the AOCC results of Zhao *et al.* [12] due to the fact that the higher endergonic channels are not included, which may be important in the relatively-high-energy region.

For electron capture to  $C^{3+}(2p)$ , there is excellent agreement between the present calculation and the only experimental data of Dijkkamp *et al.* [4]. Compared with the calculations of Errea *et al.* [9], good agreement is obtained for electron capture to the  $C^{3+}(2s)$  and  $C^{3+}(2p)$  states, especially for energy larger than 800 eV/amu, as shown in Fig. 9(a). In Fig. 9(b) the  $n,l$ -resolved SEC cross sections for electron capture to  $C^{3+}(3l)$  are compared with the only results of the AOCC calculations of Zhao *et al.* [12] and the only experimental results of Dijkkamp *et al.* [4]. The total QMOCC

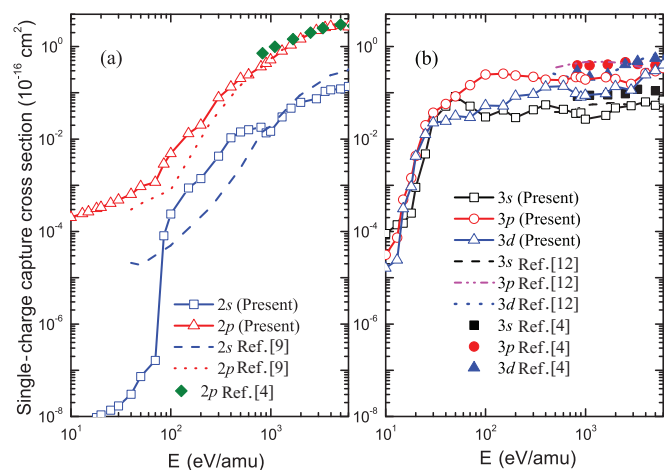


FIG. 9. (Color online) Comparison between the state-selective SEC cross sections and other theoretical and experimental results for  $C^{4+}(1s^2) + He$  collisions.

cross section seems comparable to the measured values of Dijkkamp *et al.* [4], as shown in Fig. 7; however, there is a large difference for electron populations in different  $3l$  states. The discrepancies in Fig. 9(b) are also due to the absence of higher endergonic channels in the present QMOCC calculation, which become important in the high-energy collision region and greatly affect the electron population in charge transfer processes.

## V. CONCLUSION

In the present work,  $C^{4+}(1s^2) + He$  collisions have been investigated by using the QMOCC method. The SEC and DEC cross sections have been calculated in the energy range of  $10^{-6}$ –6 keV/amu, for which the *ab initio* potential curves and nonadiabatic coupling matrix elements are computed by using the MRD-CI method. It was found that DEC dominates the electron-capture processes for  $E < 2$  keV/amu, whereas for the higher-energy region, SEC becomes more important. For the total SEC and DEC cross sections, there is good agreement between the present calculations and the available measurements and calculations, except for  $E < 0.1$  keV/amu and  $E > 3$  keV/amu. To eliminate discrepancies in the

high-energy region, more endergonic channels should be included in the QMOCC calculation and the ETF should be considered. For discrepancies in the very-low-energy region, reliable experiments and calculations are highly desired. For  $n, l$ -resolved DEC and SEC processes, good agreement has also been achieved between the present QMOCC calculations and the available results, except for electron capture to  $C^{3+}(3l)$  states. Similarly, this is due to insufficient endergonic channels having been included in the QMOCC calculations, something that needs to be further checked by future high-precision measurements.

## ACKNOWLEDGMENTS

This work was supported by the National Basic Research program of China under Grant No. 2013CB922200, the Foundation for the Development of Science and Technology of Chinese Academy of Engineering Physics under Grants No. 2012B0102015 and No. 2013A0102005, the National Science Foundation of China under Grants No. 10979007, No. 11005049, No. 11025417, No. 11179041, and No. 11204017, and the Defense Industrial Technology Development Program under Grant No. b1520110011.

- 
- [1] H. J. Zwally, D. W. Koopman, and T. D. Wilkerson, *Rev. Sci. Instrum.* **40**, 1492 (1969).
- [2] D. H. Crandall, R. E. Olson, E. J. Shipsey, and J. C. Browne, *Phys. Rev. Lett.* **36**, 858 (1976).
- [3] D. H. Crandall, *Phys. Rev. A* **16**, 958 (1977).
- [4] D. Dijkkamp, D. Čirić, E. Vlieg, A. de Boer, and F. J. de Heer, *J. Phys. B* **18**, 4763 (1985).
- [5] K. Ishii, A. Itoh, and K. Okuno, *Phys. Rev. A* **70**, 042716 (2004).
- [6] E. J. Shipsey, J. C. Browne, and R. E. Olson, *Phys. Rev. A* **15**, 2166 (1977).
- [7] M. Kimura and R. E. Olson, *J. Phys. B* **17**, L713 (1984).
- [8] R. A. Phaneuf and D. H. Crandall (unpublished).
- [9] L. F. Errea, B. Herrero, L. Méndez, and A. Riera, *J. Phys. B* **28**, 693 (1995).
- [10] L. F. Errea, B. Herrero, L. Méndez, and A. Riera, *Few-Body Syst.* **19**, 31 (1995).
- [11] J. P. Hansen, *J. Phys. B* **25**, L17 (1992).
- [12] Y. Q. Zhao, L. Liu, P. Xue, J. G. Wang, H. Tanuma, and R. Janev, *J. Phys. Soc. Jpn.* **79**, 064301 (2010).
- [13] L. Pichl, Y. Li, R. J. Buenker, M. Kimura, J. Horáček, and I. Schneider, *J. Plasma Fusion Res. Ser.* **7**, 249 (2006).
- [14] L. Pichl, R. Suzuki, M. Kimura, Y. Li, R. J. Buenker, M. Hoshino, and Y. Yamazaki, *Eur. Phys. J. D* **38**, 59 (2006).
- [15] D. Belkić, I. Mančev, and J. Hanssen, *Rev. Mod. Phys.* **80**, 249 (2008).
- [16] D. Belkić, *J. Math. Chem.* **47**, 1420 (2010).
- [17] R. J. Buenker and R. A. Phillips, *J. Mol. Struct. THEOCHEM* **123**, 291 (1985).
- [18] S. Krebs and R. J. Buenker, *J. Chem. Phys.* **103**, 5613 (1995).
- [19] D. E. Woon and T. H. Dunning, Jr., *J. Chem. Phys.* **100**, 2975 (1994).
- [20] T. H. Dunning, Jr., *J. Chem. Phys.* **90**, 1007 (1989).
- [21] R. J. Buenker and S. D. Peyerimhoff, *Theor. Chim. Acta* **35**, 33 (1974); **39**, 217 (1975); R. J. Buenker, *Int. J. Quantum Chem.* **29**, 435 (1986).
- [22] Y. Ralchenko, A. E. Kramida, and J. Reader, NIST ASD Team, NIST Atomic Spectra Database, version 4.0.1, 2010 (unpublished), available at <http://physics.nist.gov/asd>.
- [23] B. Herrero, I. L. Cooper, and A. S. Dickinson, *J. Phys. B* **29**, 5583 (1996).
- [24] B. Zygelman and A. Dalgarno, *Phys. Rev. A* **33**, 3853 (1986).
- [25] M. Kimura and N. F. Lane, *Adv. At. Mol. Phys.* **26**, 79 (1989).
- [26] B. R. Johnson, *J. Comput. Phys.* **13**, 445 (1973).
- [27] T. G. Heil, S. E. Butler, and A. Dalgarno, *Phys. Rev. A* **23**, 1100 (1981).
- [28] L. F. Errea, L. Méndez, and A. Riera, *J. Phys. B* **15**, 101 (1982).
- [29] P. C. Stancil and B. Zygelman, *Astrophys. J.* **472**, 102 (1996).
- [30] Y. Zhou, Y. Z. Qu, C. H. Liu, and X. J. Liu, *Chin. Phys. Lett.* **28**, 033401 (2011).
- [31] C. H. Liu, Y. Z. Qu, J. G. Wang, Y. Li, and R. J. Buenker, *Phys. Lett. A* **373**, 3761 (2009).
- [32] T. Iwai, Y. Kaneko, M. Kimura, N. Kobayashi, S. Ohtani, K. Okuno, S. Takagi, H. Tawara, and S. Tsurubuchi, *Phys. Rev. A* **26**, 105 (1982).